J. COMPUTATIONAL PHYSICS –EMRS-Conference 2001, PAPER Reference:A-VI.1

MICROMAGNETIC SIMULATION OF THE MAGNETIC SWITCHING BEHAVIOUR OF MESOSCOPIC AND NANOSCOPIC STRUCTURES

J. Fidler, T. Schrefl, V. D. Tsiantos, W. Scholz, D. Suess

Institute of Applied and Technical Physics, Vienna University of Technology,

Wiedner Haupstr. 8-10, A-1040 Wien, Austria.

Abstract

Magnetic switching of small particles, thins film elements and nano-wires becomes increasingly important in magnetic storage and magneto electronic devices. The magnetisation reversal processes are studied using a three dimensional hybrid finite element/boundary element micromagnetic model. Transient magnetization states during switching are investigated numerically in thin $Ni_{80}Fe_{20}$ and Co nano-elements of square (100 x 100 nm^2), rectangular (100 x 300 nm^2) and circular (100 nm diameter) shapes with a thickness of 20 nm. Switching dynamics are calculated for external fields applied instantaneously and for rotational fields with field strengths in the order of the static critical field (H_{ext}=0.02–0.32 J_s/μ_0). Reversal in the unidirectional field proceeds by the nucleation and propagation of end domains toward the centre of the particle. It is found that the switching time strongly depends on the Gilbert damping parameter α. Small values of α ($\leq$ 0.1) lead to shorter switching times at small field strength values, whereas for H_{ext}=0.6-1.0 J_s/μ_0 minimum switching times occur for large damping value α=1.0. Materials with uniaxial magneto-crystalline anisotropy, such as Co, require larger field strengths, but exhibit shorter switching times. Reversal in rotational fields involves inhomogeneous rotation of the end domains toward the rotational field direction. Depending on the damping parameter fast switching times ($\leq$ 0.1 ns) are obtained by increasing the field strength to H_{ext}=0.5 J_s/μ_0. Taking into account thermal fluctuations the reversal mechanisms of Co nano-wires were studied, and values for the activation volume and for the domain wall velocity were derived.

Keywords: Numerical micromagnetics, precessional switching, magnetic nano-elements,
Co nano-wire

Corresponding Author:
J. Fidler, Tel: +43 1 58801 13714, Fax +43 1 58801 13798;E-mail: fidler@tuwien.ac.at
Institute of Applied and Technical Physics, Vienna University of Technology, Wiedner Haupstraße 8-10, A-1040 Wien, Austria.

1. Introduction

Over recent years the investigation of the magnetic switching behaviour of ferromagnetic elements has become more advanced due to improvements in numerical micromagnetic methods and high accuracy fabrication methods, such as electron beam lithography and focused ion beam techniques. The development of advanced magnetic materials for heads and media for high density data storage, microsensor applications and magneto-mechanic devices requires a precise understanding of the magnetic switching behaviour[1,2]. The theory of micromagnetics combines Maxwell´s equations for the magnetic field with an equation of motion describing the time evolution of the magnetisation. The local arrangement of the magnetic moments follows from the complex interaction between intrinsic magnetic properties, such as the magnetic exchange and the magneto-crystalline anisotropy and the microstructure of the material. The finite element method is a highly flexible tool to describe the interaction between microstructure and magnetisation processes.

The investigation of the switching behaviour has been the subject of many recent experimental and theoretical work. Experimentally, in-situ domain observation using Lorentz electron microscopy [3], magnetic force microscopy [4] and time resolved magnetic imaging [5] provides a detailed understanding domain formation and reversal processes. The numerical solution of the Landau Lifshitz - Gilbert equation of motion provides the theoretical background for the switching process of ferromagnetic structures. The switching time considerably depends on the damping constant. Kikuchi [6] derived the difference of the minimum reversal times in a sphere and a magnetic thin film depending on the damping parameter. Leineweber and Kronmüller [7] investigated the reversal dynamics of small hard magnetic particles using a dynamic finite element method. They reported a waiting time after the application of an applied field, before the nucleation of reversed domains is initiated. Koch et al. [8] investigated the switching dynamics of micron-sized magnetic thin films experimentally and numerically. They observed switching times well below 0.5 ns. With decreasing size of the magnetic structures, thermally activated reversal process become significant. Thermally induced reversal may influence the writing process as well as the long-term stability of written bits in magnetic recording. Zhang and Fredkin [9] used the finite element method to study thermally activated reversal in ellipsoidal particles large enough to show an inhomogeneous reversal process.

Examples will be shown for the nucleation of reversed magnetic domains and the expansion of the resulting domain walls in thin patterned media used in MRAM, spin valve applications and magnetic quantum cellular automata. In the first part we present three dimensional (3D) micromagnetic simulations of the switching of Permalloy with zero anisotropy and uniaxial Co nano-elements in the presence of an unidirectional field and a rotational field with variable field strength and rotation speed. Thermal fluctuations, defects and other forms of disorder as well as eddy-currents occurring during the fast switching process are not included. Finally, in the last part we show numerical results of the thermally activated switching of Co nano-wires.

2. Micromagnetic framework

In micromagnetics the magnetic polarization is assumed to be a continuous function of space. The time evolution of the magnetization follows the Gilbert equation of motion.

$$\frac{d\mathbf{J}}{dt} = -|\gamma_0|\,\mathbf{J}\times\mathbf{H}_{eff} + \frac{\alpha}{J_s}\,\mathbf{J}\times\frac{\partial\mathbf{J}}{\partial t} \qquad (1)$$

which describes the physical path of the magnetic polarization **J** towards equilibrium. The effective field $\mathbf{H}_{\text{eff}}$ is the negative functional derivative of the total magnetic Gibb's free energy, which can be expressed as the sum of the exchange energy, the magneto-crystalline anisotropy energy, the magnetostatic energy, and the Zeeman energy [10]. The term γ_0 is the gyromagnetic ratio of the free electron spin and α is the damping constant. To solve the Gilbert equation numerically the magnetic particle is divided in finite elements.

We have used a 3D numerical micromagnetic model with tetrahedral finite elements [11] with a constant edge length of 2.5 nm and 5 nm to study thin nanostructured $Ni_{80}Fe_{20}$ and Co elements with different shapes, such as square, rectangular and dot elements with dimensions 100 x 100 x 20 nm^3, 100 x 300 x 20 nm^3, and 100 nm in diameter. The total number of the elements varied from 8157 to 94073 depending on the edge length and shape of the nano-element. The micromagnetic simulations revealed no significant difference between the calculations using the finite element edge length of 2.5 nm and 5 nm. Table 1 summarizes the typical intrinsic material parameters used for the simulations. The calculations were started after saturation parallel to the y-direction.. The instantaneous static field was applied parallel to the –y direction and the rotating magnetic field with a frequency of 10 GHz was applied in the (x,y)-plane.

A hybrid finite element boundary element method [12], is used to calculate the scalar potential u on every node point of the finite element mesh. The demagnetising field, which contributes to the effective field, is the negative derivative of the scalar potential. The effective field $\mathbf{H}_{\text{eff,i}}$ at the node point i of an irregular finite element mesh can be approximated using the box scheme

$$\mathbf{H}_{\text{eff,i}} = -\left(\frac{\delta E_t}{\delta \mathbf{J}}\right)_i = -\frac{1}{V_i}\frac{\partial E_t}{\partial \mathbf{J}_i} \quad \text{, for Vi}\rightarrow 0, \tag{2}$$

where Vi is the volume of the surrounding node i, such that

$$\sum_i V_i = V \quad \text{, and} \quad V_i \cap V_j = 0 \quad \text{for i}\neq\text{j}, \tag{3}$$

The discretization of the Gilbert equation leads to an ordinary differential equation (ODE) for every node for each component. In case of a non-stiff problem it is advisable to use an appropriate method, such as Adams, whereas in stiff problems a backward differentiation formula (BDF) method could be an option for the time integration. BDF method is implicit, so at each time step a non-linear algebraic system must be solved. For the non-linear system a method, such as Newton, has to be used which leads usually to a very large system of linear equations. In this paper the latter is solved using the scaled preconditioned incomplete generalised minimum residual method (SPIGMR) [13], based on GMRES (generalized minimum residual method) proposed by Youcef Saad [14]. SPIGMR belongs to the family of Krylov subspace methods, which are iterative methods for solving systems of linear equations, and has been explored in micromagnetics by Tsiantos et al [15,16]. The stiffness of a system can be measured by solving the system of ODEs with two different solvers, a non-stiff method (Adams) and a stiff one (BDF). If the total number of time steps (nst) taken by Adams is lower than the nst taken by BDF then the system is non-stiff. However, if nst for Adams is larger than that for BDF then the cost per time step for each method should be checked. For the Adams the main cost per time step is the function evaluation. However, for the case of BDF there is some extra cost for the linear algebra involved. This extra cost is due to linear and non-linear iterations. In general, the

preconditioned case gives faster results in terms of the non-linear and linear iterations. However, the preconditioned method roughly doubles the average cost per non-linear iteration because it computes and processes the preconditioner. Note that the simulation time has to be the same in order to have a fair comparison.

Thermal activations on a short time scale can be treated numerically adding a random thermal field to the effective field in equation (1), leading to the Langevin equation [10]:

$$\frac{d\mathbf{J}}{dt} = -|\gamma_0|\mathbf{J}\times\left(\mathbf{H}_{eff} + \mathbf{H}_{th}\right) + \frac{\alpha}{J_s}\mathbf{J}\times\frac{\partial\mathbf{J}}{\partial t}$$

At high damping the magnetization rotates more or less directly towards the field direction, as the second term in equations (3) and (4) is dominant. If the precession term becomes dominant, the polarization precesses several times around the field direction before it reaches equilibrium. Finally low damping and finite temperatures causes a random motion of the magnetization in thermal equilibrium. The resulting stochastic equation of motion describes the random motion of the magnetization in thermal equilibrium and eventually across energy barriers. The random thermal field, $\mathbf{H}_{th}$, describes the coupling of the magnetic system with a heat bath. It accounts for the interaction of the magnetic polarization with the microscopic degrees of freedom which causes the fluctuation of the magnetization distribution. The fluctuations are assumed to take place on a much faster time scale than intrinsic time scale given by the gyromagnetic ratio and the effective field. The intrinsic time scale of as given by the Gilbert equation of motion follows from the Lamor frequency

$$\omega = -\gamma\,\mathbf{H}_{\text{eff}} \tag{5}$$

The thermal field is assumed to be a Gaussian random process with the following statistical properties:

$$\left\langle H_{\text{th},i}(\mathbf{r},t)\right\rangle = 0 \tag{6}$$

$$\left\langle H_{\text{th},i}(\mathbf{r},t)H_{\text{th},j}(\mathbf{r},t)\right\rangle = D\delta_{ij}\delta(\mathbf{r}-\mathbf{r}')\delta(t-t') \tag{7}$$

The average of the thermal field vanishes taken over different realizations (4) vanishes in each direction i in space. The thermal field is uncorrelated in time and space. The strength of the thermal fluctuations follow from the fluctuation-dissipation theorem [17]:

$$D = \frac{2\alpha k_{\text{B}} T}{\gamma|\mathbf{J}|} \tag{8}$$

where k_B is the Boltzmann constant and T the temperature.

3. Effect of instantaneous field on switching

The numerical simulations were performed for different geometries and damping parameters. The quasi-static simulation with field steps of $\mu_0\Delta H$=0.02 T after saturation showed that switching occurred at the critical fields for the square, rectangular and circular dot geometries, and materials parameters, respectively. These switching fields were used for the simulations assuming the instantaneously applied field. Fig.1. compares the time evolution of the polarization of $Ni_{80}Fe_{20}$ with zero magneto-crystalline anisotropy for different damping constants. For α = 1 switching occurs only after a waiting time of about 0.6 ns for the circular dot shaped element. For α = 0.02 the waiting time reduces to about 0.4 ns for the external field strength of H_{ext}=16 KA/m (Fig.1.a). This behaviour is reversed, if the field strength is increased to 800 kA/m (Fig.1.b). Differences in minimum switching times depending on the damping parameter were also found by Kikuchi [6] investigating

the reversal times of a single domain sphere and a single domain and ultra- thin film.. Fig.2 compares the switching times ($<J_y>=0$) of the circular $Ni_{80}Fe_{20}$ dot for various damping parameters and external field strength. The transient magnetization states of Figs. 3 and 4 show that for small switching fields inhomogeneous magnetization rotation processes are dominant, whereas for a large field strength complex, inhomogeneous reversal processes (small damping parameter α) and nucleation and expansion of reversed domains (large α) are responsible for the different switching rates. The influence of the uniaxial magneto-crystalline anisotropy parallel to the external field direction leads to reduced switching times. The switching time of a circular Co dot is reduced to values less than 0.2 ns (Figs. 5 and 6) and depends again on the external field strength and the damping constant α. The shortest switching times occur, when the reversal process is controlled by the nucleation and expansion of reversed domains. These regions are clearly observed in the simulated images of Figs. 7a, 8a and 8b. For large damping-and small external field values the Zeeman energy contribution is not sufficient to overcome the large dipolar fields and leading to relatively large switching times.

Fig. 9 shows the nucleation and expansion of reversed domains within a square $Ni_{80}Fe_{20}$ and Co element with dimensions 100 x 100 x 20 nm^3 during the magnetization reversal at a constant reversed field of H_{ext}= 160 and 280 kA/m parallel to the –y-direction, respectively. For α=0.1 τhe elements switch by nonuniform rotation in 0.17 ns and 0.30 ns, respectively. The magnetization reversal process started in the $Ni_{80}Fe_{20}$ element at the corners, and the expansion of the domains followed along the edges of the square element (Fig. 9a). In contrary to $Ni_{80}Fe_{20}$ the reversal starts in the square Co element by forming of reversed domains at the opposite faces in order to reduce the local stray field (Fig. 9b). The numerical simulations show that the switching behaviour is strongly influenced by the geometry of the nano-element. The magnetization reversal of the rectangular shaped nano-element with dimensions 100 x 300 x 20 $nm^3$is found to proceed in a very similar way as in the square element. In the instantaneously applied, unidirectional field the switching starts whether by inhomogeneous rotation inside the $Ni_{80}Co_{20}$ element after nucleation at the corners of the element (Fig. 10b) or after nucleation at opposite corners in the Co element (Fig. 10b). The switching times vary from 0.15 ns for $Ni_{80}Fe_{20}$ to 0.38 ns for Co.

4. Effect of rotational field on reversal process

Under the influence of a constant, rotating field the magnetization tries to follow the external field direction and starts to rotate near the flat ends of the square reducing the magnetostatic energy (Fig. 11b), followed by the reversal of the centre. In the case of very fast switching and small field strength (H_{rot}=160 kA/m/10 GHz for $Ni_{80}Fe_{20}$ and H_{rot}=280 kA/m/10 GHz for Co) the magnetization of only small regions inside the nano-element is able to follow the external field direction. Complex magnetization distributions within the nano-element occur (Fig. 12b). Figs. 11a and 12a show that after 10 cycles of field rotation the total polarization decreases, thus the square element becomes demagnetised. The phase shift between polarization and external field vectors is rather small for zero magneto-crystalline anisotropy (Fig.11a).

Incoherent magnetization rotation occurs inside the square, if the field strength is increased to 0.50 J_s/μ_0 at 10 GHz (Fig.13b). This results for the Co square in about 95% alignment of the polarization parallel to the rotating field and a slight phase shift between the external field and the total polarization vector (Fig. 13a). The angle between the rotating field vector and the total polarization vector increases for large damping constant α= 1.

Micromagnetic simulations of the magnetization reversal show that the inhomogeneous rotation in a rotational field also leads to partial flux-closure structures and therefore facilitates the switching by reduced switching times.

5. Reversal process in nano-wires

The nucleation and reversal of reversed domains in magnetic nano-wires was studied at finite temperatures and taking into account thermal fluctuations. The energy barriers and the activation volume were derived from the numerical results. The diameter of the wire Co wire was 2 nm. A Gilbert damping constant $\alpha = 1$ was used for the calculations. The magneto-crystalline anisotropy direction was assumed to be parallel to the long axis of the wire. Wires with a length smaller than 16 nm were found to reverse by uniform rotation. Fig. 14 shows the schematics of the energy barrier as a function of the angle with respect to the easy axis. An external field lowers the energy barrier. From the calculated relaxation time, τ, the energy barrier can be derived numerically fitting the numerical results to

$$\tau = f_0^{-1} \exp\left(\frac{E_B}{k_B T}\right) \qquad (9)$$

where f_0 is the attempt frequency. The energy barrier increases with increasing volume of the wire as long as the reversal mode is uniform rotation. The numerically derived energy barrier for uniform rotation agrees well with the result obtained from the Stoner-Wohlfarth theory [18]

$$E_B(H_{ext}) = KV\left(1-\frac{H_{ext}}{H_K}\right)^2, \quad H_K = \frac{\mu_0 2K}{M_s} \qquad (10)$$

where K is the effective anisotropy constant taking into account the magneto-crystalline anisotropy and the shape anisotropy of the wire.

The simulations show that the wires with a length of 32 nm reverse by the nucleation and expansion of reversed domains. Now the energy barrier is independent of the wire length, since the nucleation process starts at the wire ends where a strong demagnetising initiates magnetization reversal. Once the reversed domain has formed, it expands over the entire wire. Fig. 15 illustrates this process. An effective activation volume, v, can be derived from the energy barrier under the assumption that the activation energy corresponds to the energy of the nucleus of reverse magnetization [18]

$$E_B(H_{ext}) = -v\mu_0 M_s H_{ext} \qquad (11)$$

The activation volume can be derived from the slope of the $E_B(H_{ext})$ curve

$$v = -\frac{1}{\mu_0 M_s}\frac{\partial E_B}{\partial H_{ext}} \qquad (12)$$

Fig. 16 gives the calculated energy barrier for a 1:16 aspect ratio nano-wire as a function of the external field. The dashed line corresponds to the analytical result obtained by Braun [19]. The numerical values for the energy barrier are about factor of 2-3 smaller then those derived analytically. This may be attributed to inhomogeneous magnetic states which neglected in the analytical model. The numerically obtained energy barrier depends linearly on the applied field which indicates that the reversal takes place by the formation of a nucleus of reverse magnetization. The magnetization reversal starts within a finite volume at the end of one wire. The activation volume was derived to be $v = (2.1\ nm)^3$

which approximately corresponds to the cube of the wire diameter. Li et al. [20]obtained a similar result from magnetic measurements on α-Fe nano-wires.

6. Conclusions

In mesoscopic and nanostructured magnets the switching fields and times which are in the order of pico- to nanoseconds are controlled by the choice of the geometric shape of the magnets, the intrinsic properties and the orientation and strength of the applied field. Understanding and controlling the magnetic switching dynamics of magnetic particles is the major challenge for technological applications. Micromagnetic modelling of the magnetization reversal process of meso- and nanoscopic elements show that the dynamics of the switching behaviour in an instantaneously applied, unidirectional field differs from the one in a rotating field, especially at high frequencies. Comparing the transient magnetization states during reversal and the switching time of Permalloy and Co elements, faster switching is obtained in materials with uniaxial anisotropy neglecting eddy current effects. The shape and the Gilbert damping parameter determine the critical switching field and time. Thermally activated processes play a significant role during the magnetization reversal of elongated Co-nanowires.

Acknowledgements

This work was supported by the Austrian Science Fund (P13260-TEC and Y-132 PHY).

References

[1] G.A. Prinz, J. Magn. Magn. Mat. 200 (1999) 57.
[2] B.D. Terris, L. Folks, J.E.E. Baglin, A.J. Kellock, H. Rothuizen, P. Vettinger, Appl. Phys. Lett. 75 (1999) 403.
[3] K. J. Kirk, J. N. Chapman, C. D. W. Wilkinson, Appl. Phys. Lett. 71 (1997) 539.
[4] E.D. Dahlberg, J.G. Zhu, Physics Today 48 (1995) 34.
[5] C. H. Back, J. Heidmann, J. McCord, IEEE Trans. Magn. 35 (1999) 637.
[6] R. Kikuchi, J. Appl. Phys. 27 (1956) 1352.
[7] T. Leineweber, H. Kronmüller, J. Magn. Magn. Mater. 192 (1999) 575.
[8]. R. H. Koch, Phys. Rev. Lett. 81 (1998) 4512.
[9] K. Zhang, D. R. Fredkin, J. Appl. Phys. 85 (1999) 5208.
[10] W. F. Brown, Jr., Micromagnetics (Wiley, New York, 1963)..
[11] J. Fidler, T. Schrefl, J. Phys. D, 33 (2000). R135.
[12] D. R. Fredkin, T. R. Koehler, IEEE Trans. Magn. 26 (1990). 415.
[13] P. N. Brown, A. C. Hindmarsh, J. Appl. Math. Comp. 31 (1989). 40.
[14] Y. Saad, M. H. Schultz, SIAM J. Sci. Stat. Comp. 7 (1986). 856.
[15] V. D. Tsiantos, J. J. Miles, B. K. Middleton, 3rd European Conference on Numerical Mathematics and Advanced Applications (ENUMATH '99), Jyväskylä, 743-752, (1999), edited by P. Neittaanmaki et al, World Scientific, Singapore, (2000).
[16] V.D. Tsiantos, D. Suess, T. Schrefl, J. Fidler, J. Applied Physics 89 (2001) 7600.
[17] J. L. Garccia-Palacios, F. J. Lazaro, Phys. Rev. B 58 (1998) 14937.
[18] R. Street, D. C. Crew, IEEE Trans. Magn. 35 (1999) 4407.
[19] H.-B. Braun, J. Appl. Phys. 76 (1994) 6310.
[20] Li, F. L., R. M. Metzger, W. D. Doyle, IEEE Trans. Magn. 33 (1997). 4423.

Table 1
Typical intrinsic material parameters used for the simulations, with J_s as saturation polarization, K_1 and K_2 as magneto-crystalline anisotropy constants and A as exchange constant.

Material	J_S [T]	K_1 [MJ/m^3]	K_2 [MJ/m^3]	A [pJ/m]
$Ni_{80}Fe_{20}$	1.00	0	0	13
Co*	1.76	0.45	0.15	13

* assuming uniaxial magneto-crystalline anisotropy parallel to the y-axis

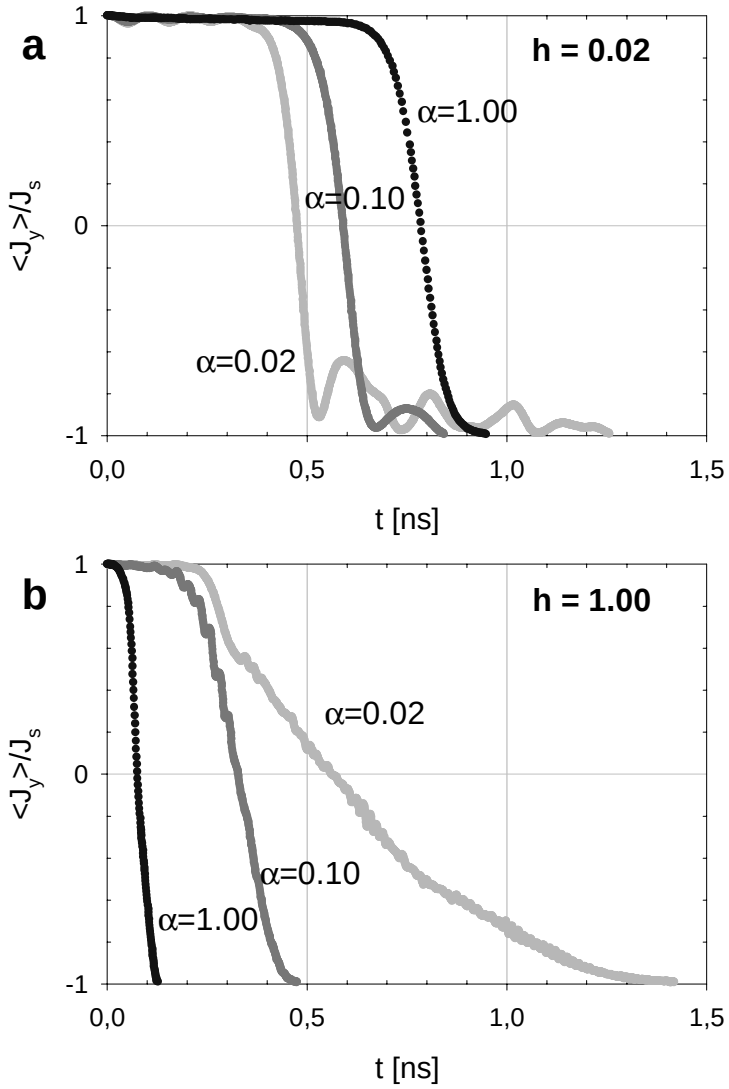

Fig.1. Time evolution of the polarization during switching of a circular $Ni_{80}Fe_{20}$ dot with 100 nm in diameter and 20 nm thickness. (a) H_{ext}=16 kA/m (h=0.02 J_s/μ_0), (b) H_{ext}=800 kA/m (h=1.00 J_s/μ_0)

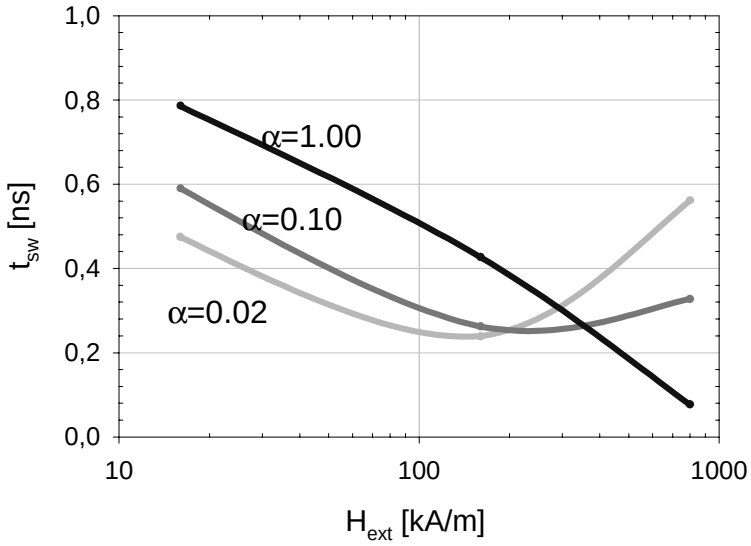

Fig. 2. Switching times of the circular $Ni_{80}Fe_{20}$ dot for various damping parameters and external field strength

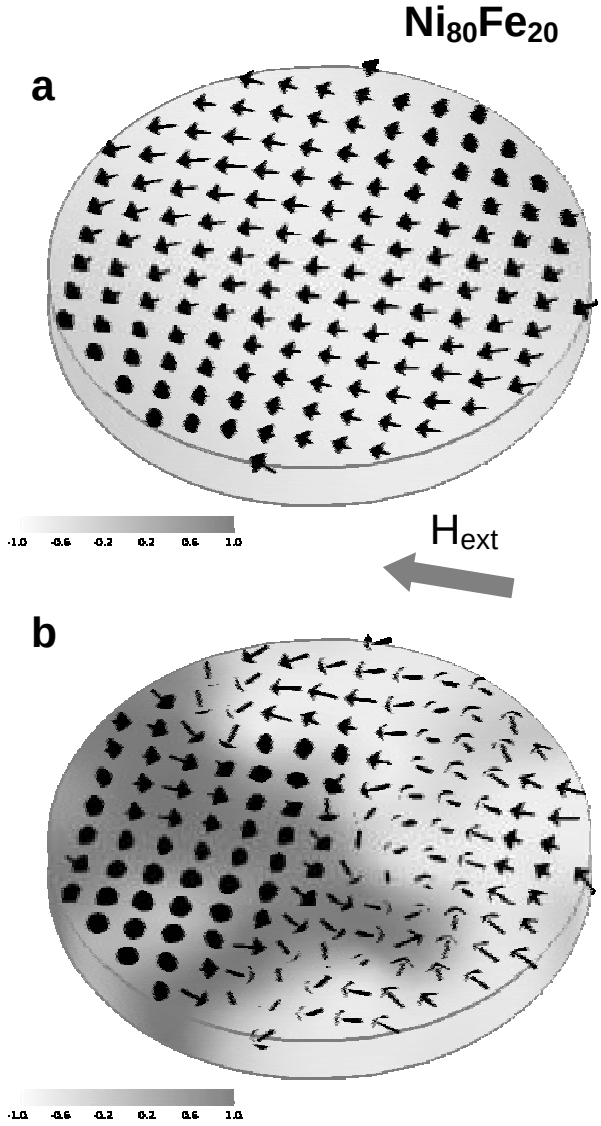

Fig. 3. Transient magnetization states within the circular Ni80Fe20 dot during the reversal process for□=0.02, (a) Hext=16 kA/m (h=0.02 Js/μ0), (b) Hext=800 kA/m (h=1.00 Js/μ0), The arrow points towards the instantaneously applied field direction (-y direction)

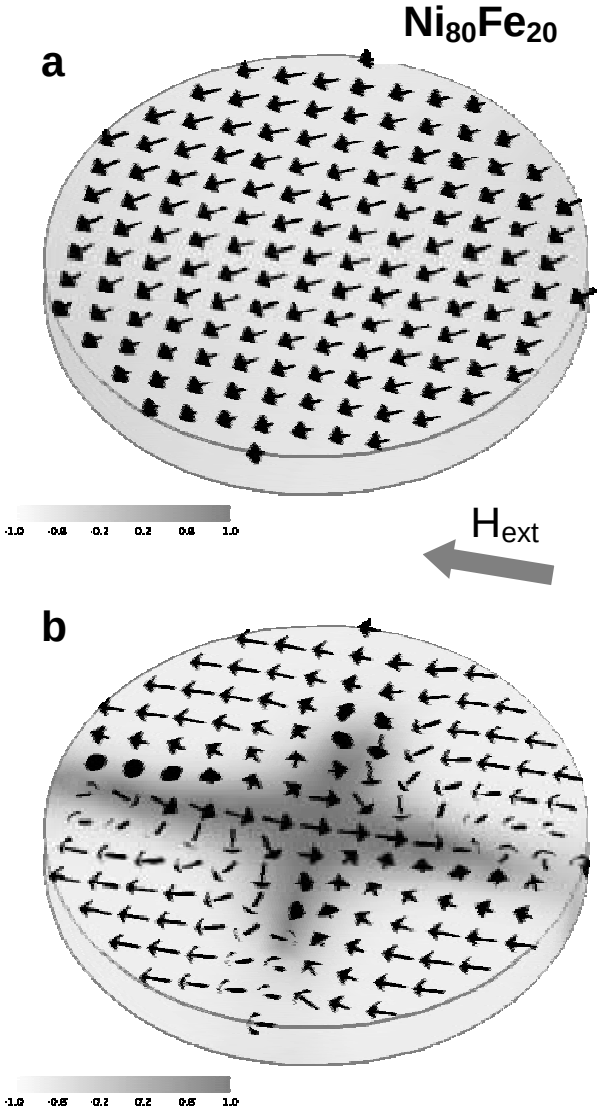

Fig. 4. Transient magnetization states within the circular Ni80Fe20 dot during the reversal process for □=1.00, (a) Hext=16 kA/m (h=0.02 Js/μ0), (b) Hext=800 kA/m (h=1.00 Js/μ0)

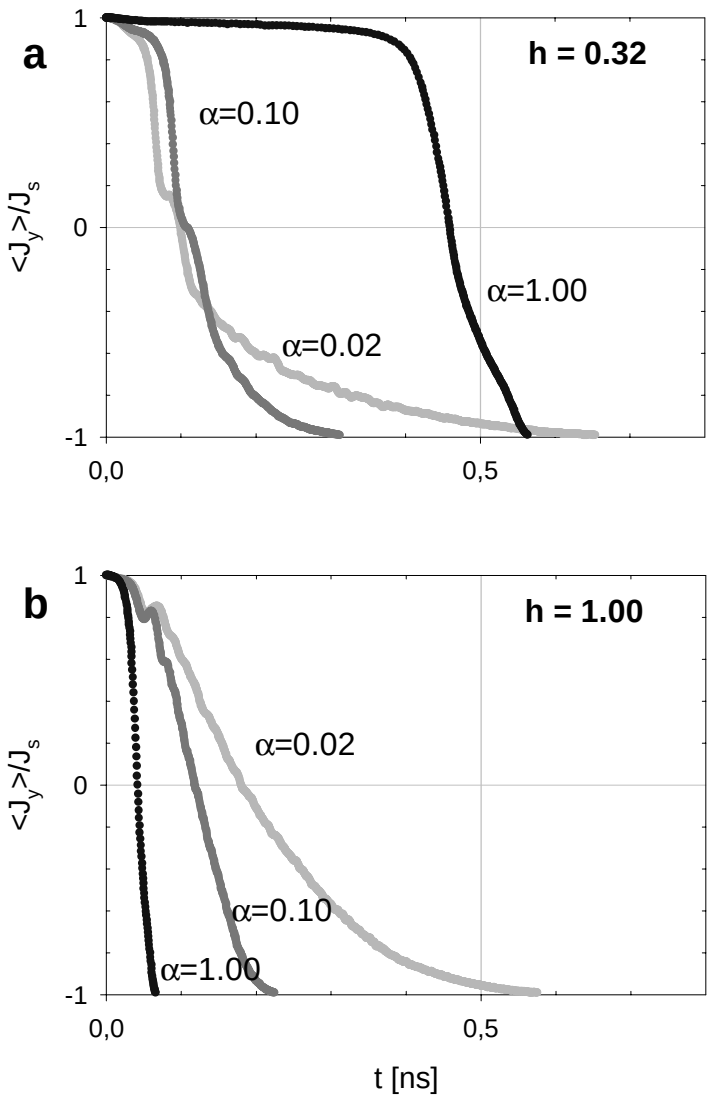

Fig. 5. Time evolution of the polarization during switching of a circular Co dot with 100 nm in diameter and 20 nm thickness, (a) Hext=450 kA/m (h=0.32 Js/μ0), (b) Hext=1400 kA/m (h=1.00 Js/μ0)

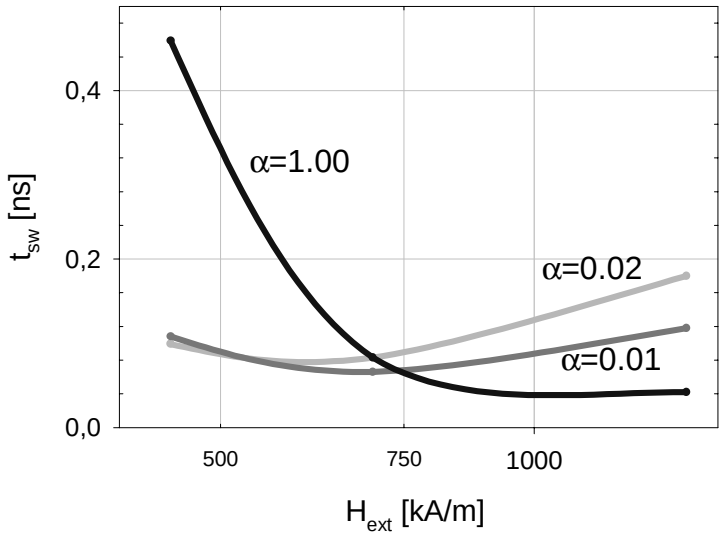

Fig. 6. Switching times of the circular Co dot for various damping parameters and external field strength

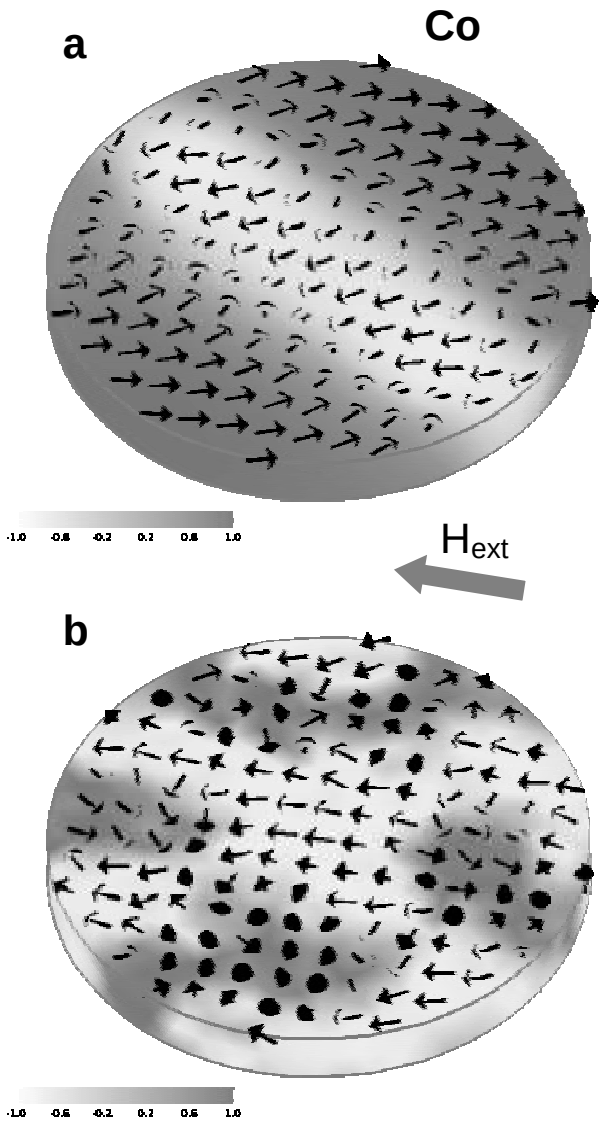

Fig. 7. Transient magnetization states within the circular Co dot during the reversal process for □=0.02, (a) Hext=450 kA/m (h=0.32 Js/μ0), (b) Hext=1400 kA/m (h=1.00 Js/μ0)

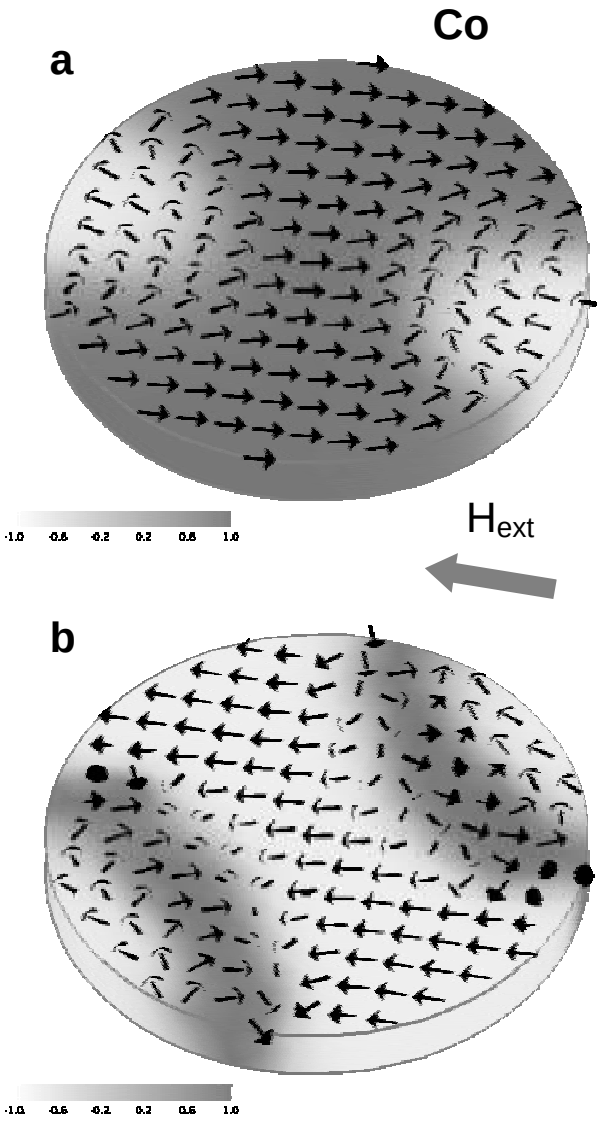

Fig.8. Transient magnetization states within the circular Co dot during the reversal process for □=1.00, (a) Hext=450 kA/m (h=0.32 Js/μ0), (b) Hext=1400 kA/m (h=1.00 Js/μ0)

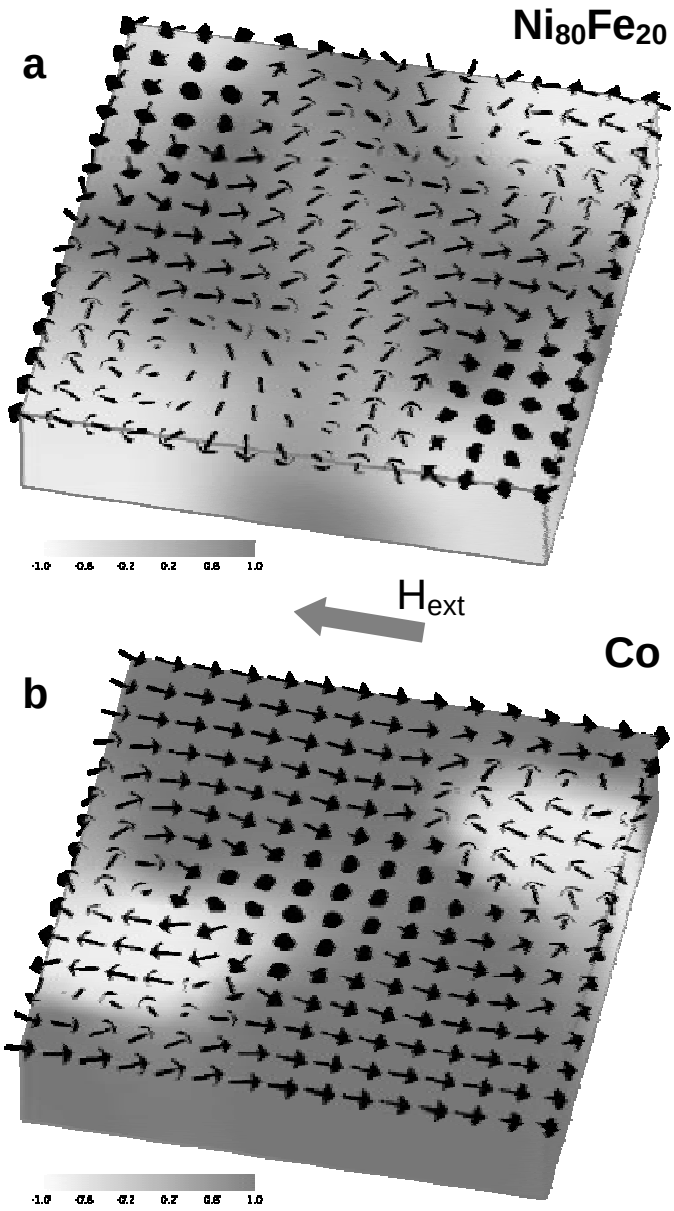

Fig. 9. Nucleation and expansion of reversed domains within a square element with dimensions 100 x 100 x 20 nm3 during the magnetization reversal in an instantaneously applied field for □=0.10, (a) Ni80Fe20, Hext=160 kA/m (h=0.20 Js/μ0), (b) Co, Hext=280 kA/m (h=0.20 Js/μ0)

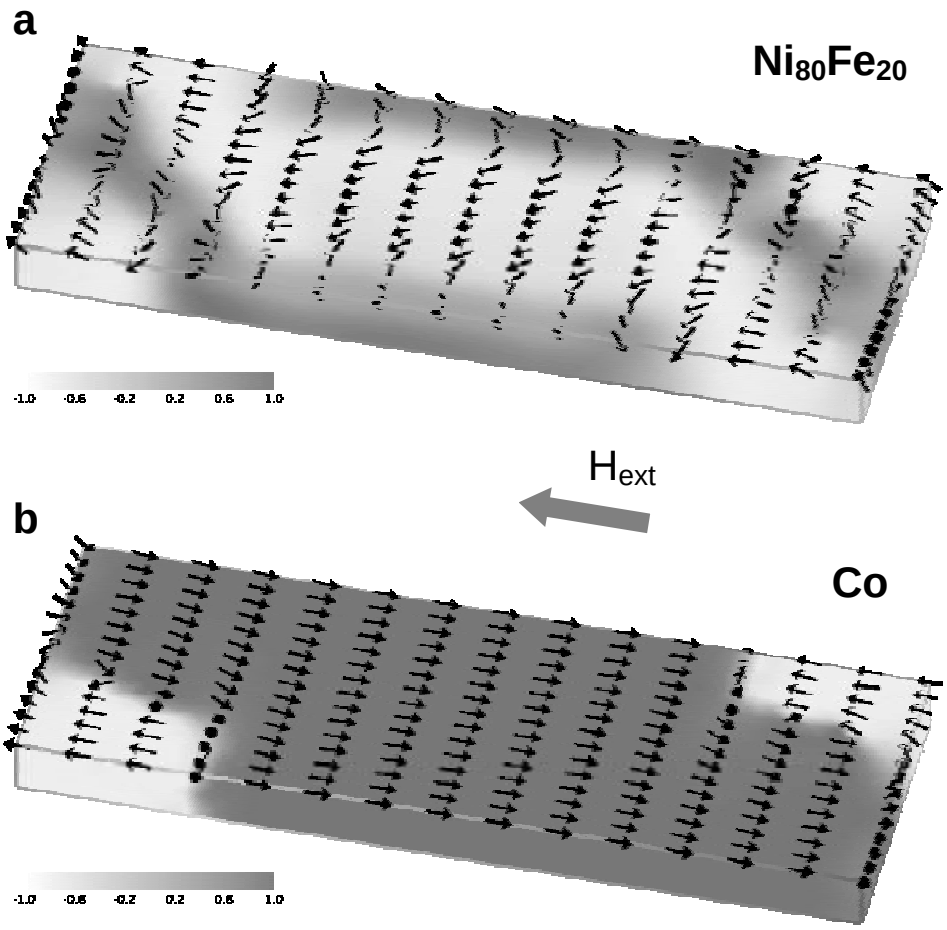

Fig. 10. Nucleation and expansion of reversed domains within a rectangular element with dimensions 100 x 300 x 20 nm3 during the magnetization reversal in an instantaneously applied field for □=0.10, (a) Ni80Fe20, Hext=160 kA/m (h=0.20 Js/μ0, (b) Co, Hext=310 kA/m (h=0.22 Js/μ0)

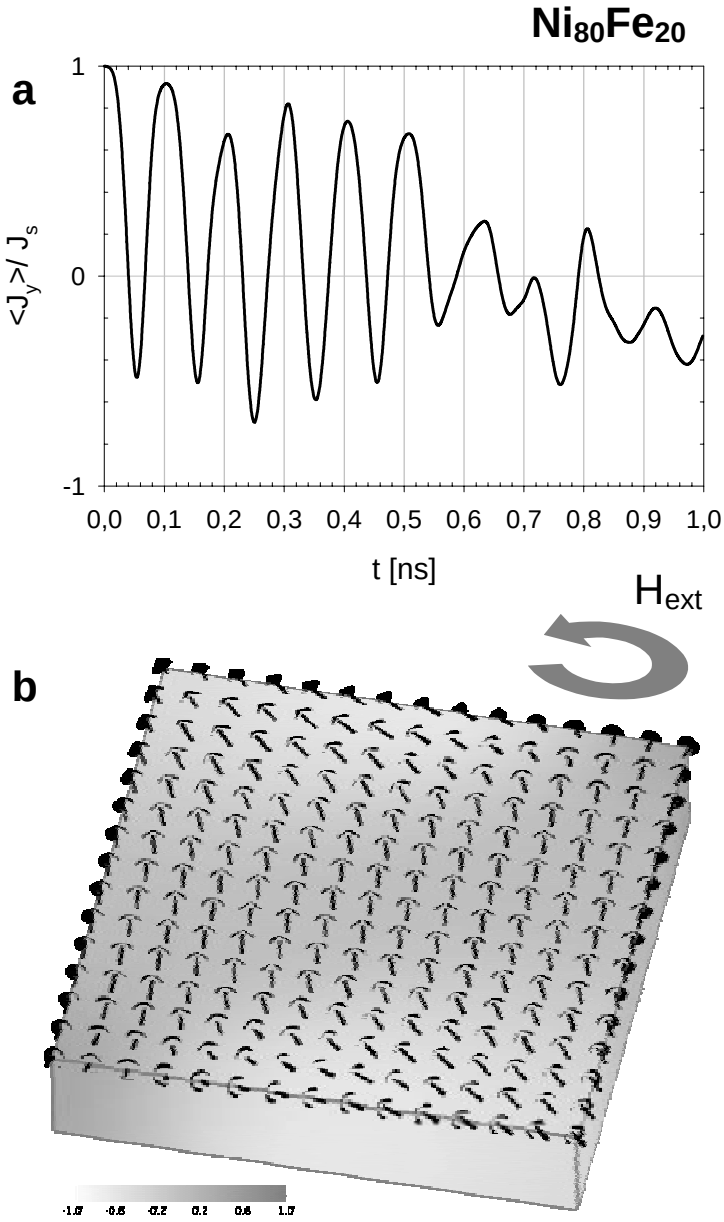

Fig.11. Time evolution of the polarisation during the application of a rotating field at 10 GHz (a) and inhomogeneous magnetization rotation (b) at t=0.05 ns inside the Ni80Fe20 square element at Hext=160 kA/m (h=0.20 Js/μ0) for □= 0.10

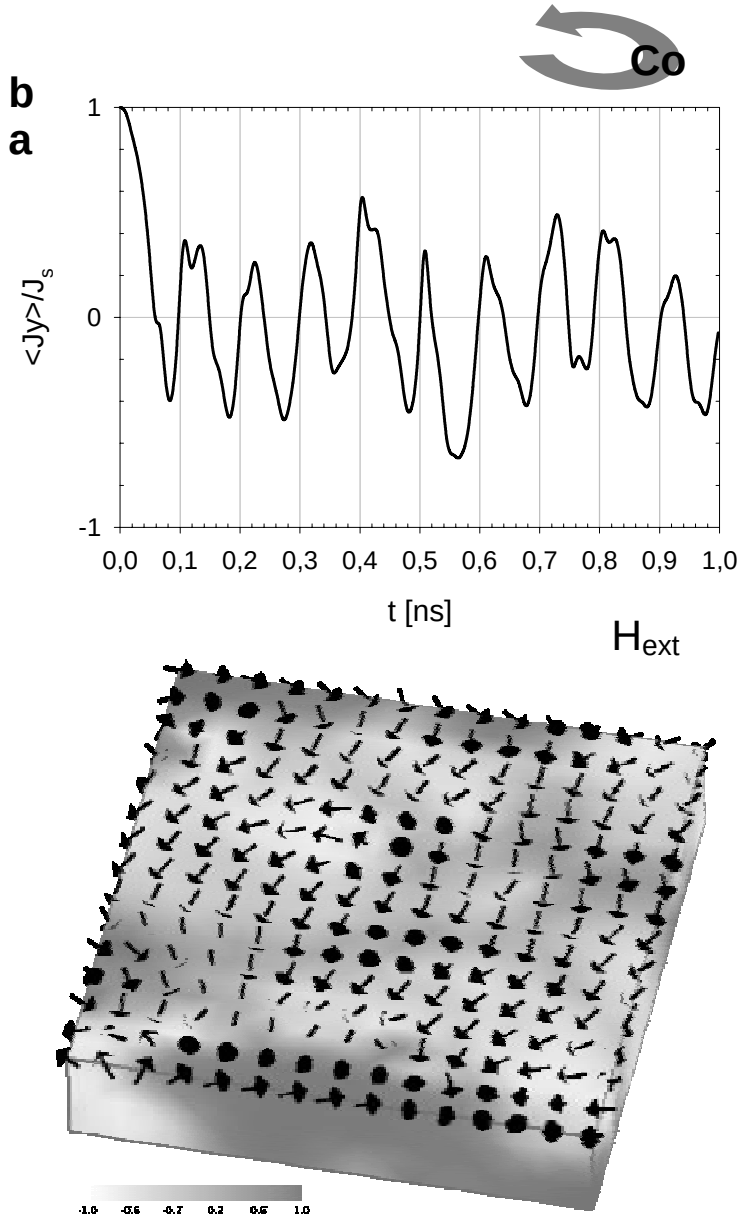

Fig. 12. Time evolution of the polarisation during the application of a rotating field at 10 GHz (a) and complex magnetization distribution (b) at t=0.07 ns inside the Co square element at Hext= 280 kA/m (h=0.20 Js/μ0) for □ = 0.10

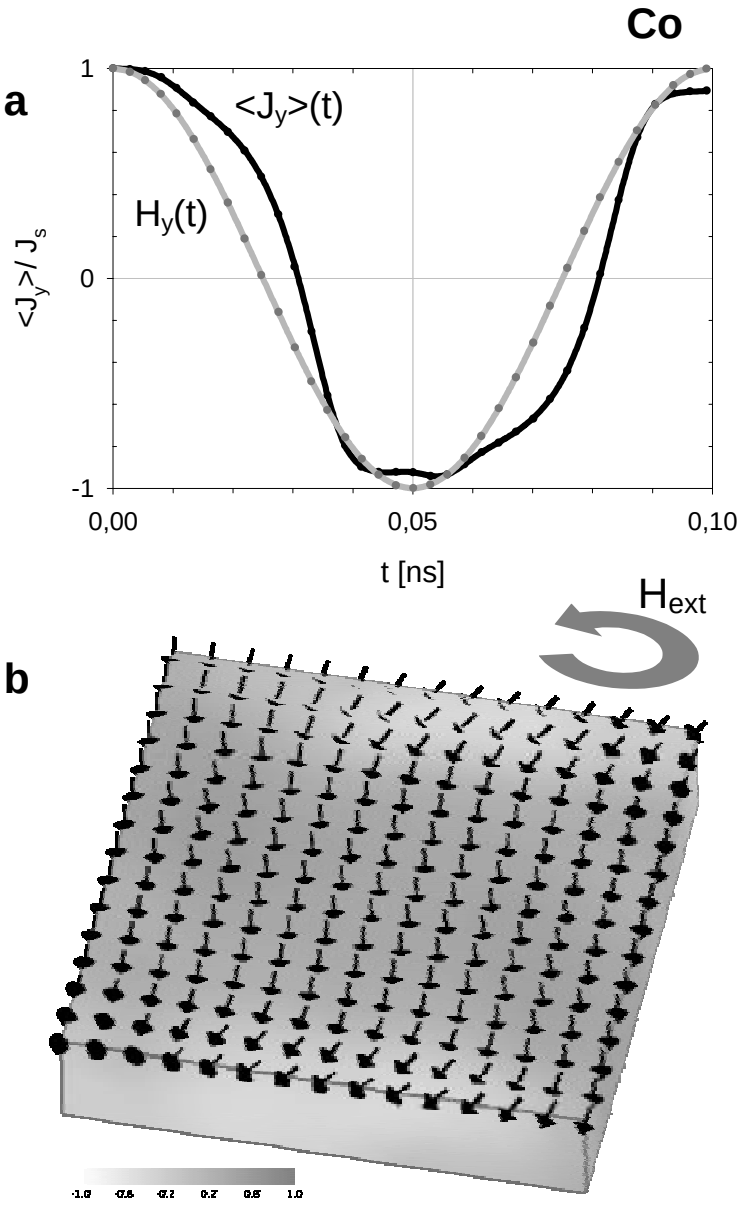

Fig. 13. Time evolution of the polarisation during the application of a rotating field at 10 GHz and external field component (a) and incoherent magnetization rotation (b) at t=0.08 ns inside the Co square element at Hext= 700 kA/m (h=0.50 Js/μ0) for □ = 0.10

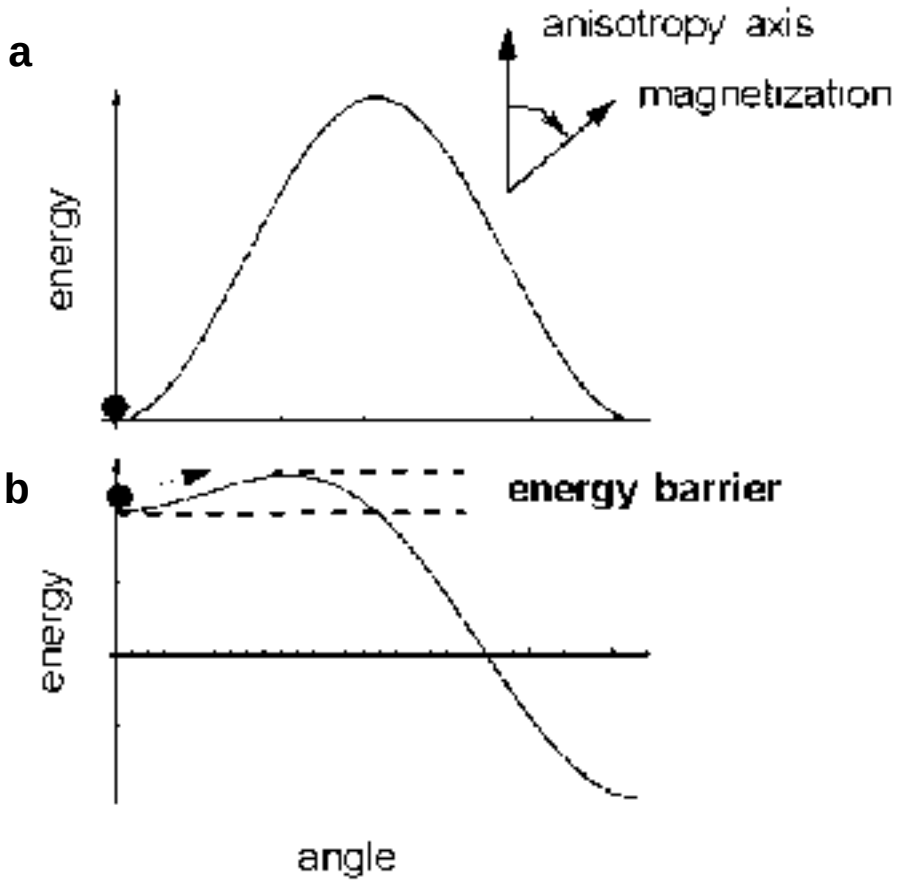

Fig. 14. Energy of a small particle as a function of the angle between the easy axis and the magnetization. (a) zero external field and (b) reversed applied field

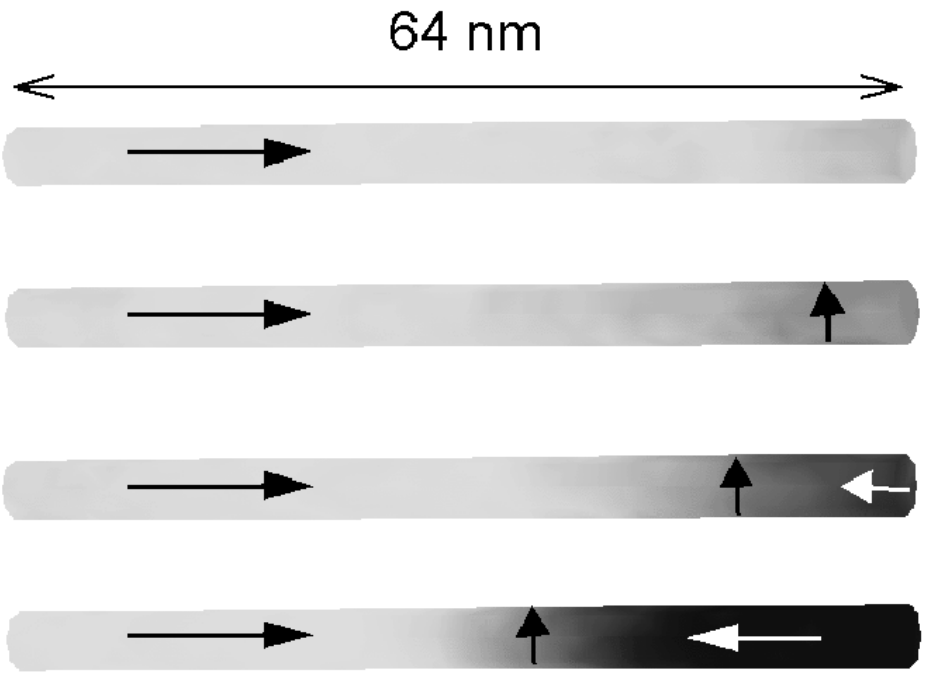

Fig. 15. Nucleation and expansion of reversed domains in Co nano-wires with an aspect ration of 1:16

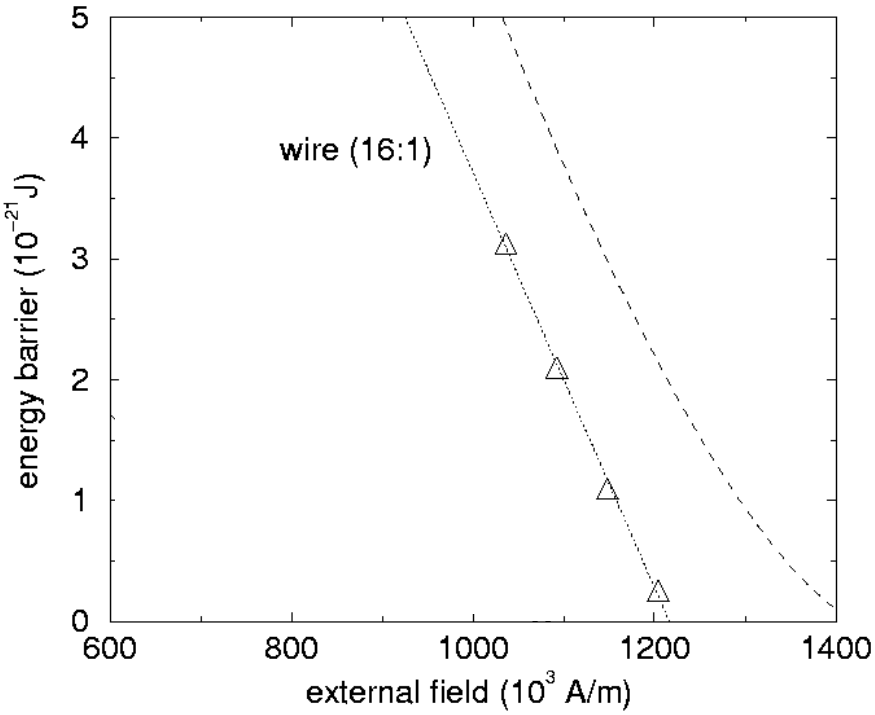

Fig. 16. Energy barrier as a function of the applied field. The open symbols give the numerical values. The dotted line is a linear fit of the numerical values.
The dashed line gives the analytic result according to Braun [19]